

# Transverse and z-Direction CVN Impact Tests of X65 Line Pipe Steels of Two Centerline Segregation Ratings



LIHONG SU, HUIJUN LI, CHENG LU, JINTAO LI, LEIGH FLETCHER,  
IAN SIMPSON, FRANK BARBARO, LEI ZHENG, MINGZHUO BAI,  
JIANLAN SHEN, and XIANYONG QU

Centerline segregation occurs as a positive concentration of alloying elements in the mid-thickness region of continuously cast slab. Depending upon its severity, it may affect mechanical properties and potentially downstream processing such as weldability, particularly for high-strength line pipe. The segregation fraction in continuously cast slabs and corresponding hot-rolled strips was assessed on API 5L grade X65 line pipe steels with different levels of segregation, rated as Mannesmann 2.0 and 1.4. The results showed that the segregation fraction in hot-rolled strip samples was in accordance with that assessed in the cast slabs, and the segregated regions in hot-rolled strip samples were found to be discontinuous. Transverse and z-direction CVN impact tests were conducted on the two strips and the results showed that centerline segregation does have an influence on the Charpy impact properties of line pipe steel. Specimens located at segregated regions exhibited lower Charpy impact toughness and strips rolled from slabs with higher segregation levels are more likely to exhibit greater variability in Charpy impact toughness. The influence of centerline segregation on z-direction Charpy impact toughness is more severe than on transverse Charpy impact toughness. Lower Charpy impact toughness and brittle fracture surface with cleavage facets along with rod-shaped MnS inclusions were observed for the strip rolled from slab with 2.0 segregation rating if the Charpy specimens were located at segregated regions. The influence on Charpy impact toughness can be associated with the pearlite structure at the centerline and level of MnS inclusions.

DOI: 10.1007/s11661-016-3578-4

© The Minerals, Metals & Materials Society and ASM International 2016

## I. INTRODUCTION

CENTRELINE segregation appears as areas of concentrated solutes in the mid-thickness region of continuously cast steel slabs.<sup>[1]</sup> Using techniques such as sulfur printing or macro-etching, centerline segregation can be observed as dark dots, segments, or lines in the mid-thickness region of a transverse section of steel slabs.<sup>[1]</sup> If it is severe, centerline segregation may have an influence on the properties of the plates or strips rolled from the slabs and then as a consequence on the performance of line pipes.<sup>[2]</sup>

The influence of centerline segregation in the cast slab, on final product performance, will be dependent upon

the size and dispersion of the pockets of segregation. Local regions of elemental segregation increase hardenability and may lead to undesirable microstructures such as martensite during the welding of the pipe. The consequences of such microstructures are increased hardness and susceptibility to hydrogen-assisted cold cracking (HACC). Traditionally, the severity of centerline segregation was assessed by the so-called “Mannesmann standard,”<sup>[3]</sup> of which the segregation ratings are scaled from level 1 to 5 and the size and proportion of segregation features increases with the ratings. It is therefore assumed that the influence of centerline segregation on the properties of final product would be more severe for slabs with higher segregation ratings.

There have been many reports showing that centerline segregation can have a deleterious effect on mechanical properties such as Charpy impact toughness of rolled plates or strips.<sup>[4–9]</sup> However, the influence of different levels of centerline segregation on the mechanical properties of line pipe has not been adequately quantified with respect to slab segregation ratings. The most related work was published by Gray in Reference 10 where he reported the influence of four different levels of centerline segregation on the hardness in segregated bands of corresponding pipes and found that the hardness in segregated bands of pipes increased with increasing segregation level of slabs.

---

LIHONG SU, Research Fellow, HUIJUN LI and FRANK BARBARO, Professors, CHENG LU, Associate Professor, JINTAO LI, Ph.D. Candidate, and LEIGH FLETCHER and IAN SIMPSON, Industry Advisors, are with the School of Mechanical, Materials and Mechatronics Engineering, University of Wollongong, Wollongong, Australia. Contact e-mail: lihongsu@uow.edu.au LEI ZHENG, Chief Researcher, and MINGZHUO BAI, Researcher, are with the Baosteel Research Institute, Baoshan Iron & Steel Co., Ltd., Shanghai, China. JIANLAN SHEN, Engineer, is with the Manufacturing Department, Baoshan Iron & Steel Co., Ltd., Shanghai, China. XIANYONG QU, Engineer, is with the Department of Tube Making, Baoshan Iron & Steel Co., Ltd., Shanghai, China.

Manuscript submitted October 8, 2015.

Article published online June 2, 2016

Reference 9 reported ferrite/pearlite bands at centerline segregation region and claimed that these structures were responsible for delamination and lower Charpy impact energy. Delamination was often observed on the fracture surface of transverse Charpy specimens and was usually associated with a plane parallel to the rolling plane. There are various reasons for the delamination of this plane including the existence of martensite bands, pearlite bands, or other structures.<sup>[11,12]</sup> During transverse Charpy tests, these banded structures were not the main fracture plane. In order to observe the behavior of these banded structures more in detail, *z*-direction Charpy tests are a better technique, as in this type of deformation the structure parallel to the rolling plane would be the main fracture plane.

*Z*-direction (or through-thickness as used in some references) Charpy *v*-notch (CVN) impact tests have not often been reported much for line pipe steel. Reference 11 reported transverse and *z*-direction Charpy transition curves for 3Cr12 plate and the results showed that for plates with banded structure, severe splitting and delamination was observed at transverse Charpy fractured surfaces and the Charpy transition temperature for *z*-direction samples was significantly higher than that of transverse samples. Brittle cleavage fracture characteristics were observed on certain areas of the fracture surface of *z*-direction samples, but detailed fracture surface images were not presented. Reference 13 investigated the delamination behavior of four classes of HSLA steels through longitudinal, transverse, and *z*-direction (through-thickness) mechanical testing and through-thickness embrittlement was observed. It was stated that the delamination fracture followed a critical stress criterion and the through-thickness embrittlement might be induced by the dimensional anisotropy microstructure: polygonal or acicular ferrite or prior austenite. The presence of flattened MnS inclusions and the crystallographic texture component {100} might also contribute to the embrittlement but was not essential.

In the current work, CVN impact tests in both transverse and *z*-direction were conducted on line pipe steel strips hot rolled from slabs with two different segregation levels in order to investigate the influence of centerline segregation on Charpy impact properties.

## II. EXPERIMENTAL

X65 grade line pipe steels were provided by Baoshan Iron & Steel Co., Ltd. for use in this work. Slab samples for evaluation of centerline segregation were taken from the head part of the first slab from a cast, and hot-rolled strips were taken from the head part of the relevant coil. This sampling regime for strips and slabs from

neighboring regions was chosen in the attempt to match segregation severity and distribution. The slab thickness was 230 mm and the strip thickness was 9.4 mm. Steels of two different chemical compositions (listed in Table I) were investigated and were named #1 and #2, respectively.

Centerline segregation of the cast slabs was evaluated on the slab images after macro-etching with 50 pct HCl at 343 K (70 °C) using a self-developed assessment method.<sup>[14,15]</sup> Based on the Mannesmann rating scale,<sup>[3]</sup> the segregation levels for slabs #1 and #2 are equivalent to 2.0 and 1.4, respectively. The transverse cross-section of the rolled strip was sectioned to small pieces and then polished and etched using 2.5 pct nital solution to observe the segregation features after rolling.

Transverse CVN impact tests were conducted using subsize specimens of dimensions 10 × 7.5 × 55 mm, machined according to ISO 148-1 standard<sup>[16]</sup> from the hot-rolled strips with the long direction parallel to transverse direction of the strip. *Z*-direction CVN impact tests were conducted on the hot-rolled strips using full-size specimens of dimensions 10 × 10 × 55 mm. *Z*-direction CVN specimens were prepared by stud welding of extensions of two pieces of sacrifice materials to the top and bottom surfaces of a transverse section of the hot-rolled strips. The specimen orientation and notation is shown in Figure 1(a). Figure 1(b) shows a welded *z*-direction Charpy specimen.

Because the segregated regions are discontinuous in the rolled strip, the Charpy specimens' notch may or may not be located at regions with segregation features. This chance event is illustrated in Figure 2.

CVN impact tests were conducted at 293 K (20 °C) on an Instron MPX750 Impact test machine with a capacity of 750 J using a 2-mm-radius ISO striker. The fracture surfaces of Charpy specimens were characterized using a JEOL JSM-7001F field emission gun scanning electron microscope (SEM) equipped with energy-dispersive X-ray spectroscopy (EDS).

Vickers micro-hardness of the segregation band and the metal matrix was measured with a Leco hardness testing machine using a load of 10 g and a dwell time of 12 seconds. This load was selected to ensure a relatively small indent size. When measuring the hardness of the segregation band, the indentation was taken at selected thick segregation bands to ensure that the indents fully fit inside the segregation bands, otherwise the measurement was considered invalid. The hardness of the metal matrix was measured at the quarter-thickness of the strips. A total of 10 measurements were taken to obtain the average value. It should be noted that there could be a possible sampling effect especially for strip #2 mentioned below because the segregation band in this strip is composed of scattered pearlite pockets.

**Table I. Chemical Composition of the Investigated Steels (Weight Percent)**

Steel	C	P	Mn	Si	S	Ni	Cr	Mo	Cu	Al	Ca	N	Nb	Ti
#1	0.044	0.014	1.52	0.18	0.002	0.006	0.016	0.096	0.009	0.041	0.0013	0.005	0.039	0.016
#2	0.031	0.007	1.50	0.19	0.002	0.006	0.015	0.097	0.007	0.026	0.0016	0.0035	0.041	0.018

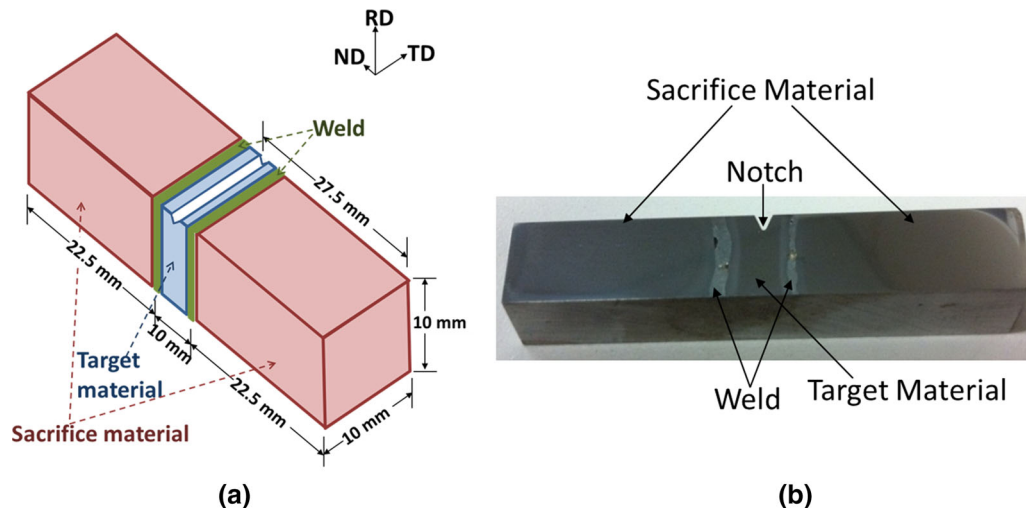


Fig. 1—(a) Schematic illustration and (b) real photo of *z*-direction Charpy specimen prepared by stud welding.

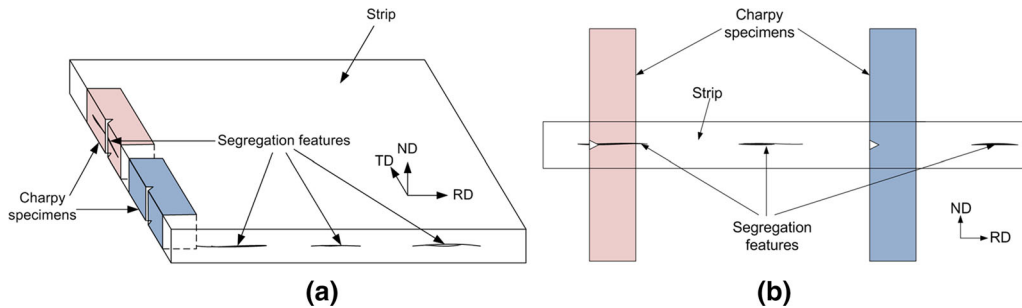


Fig. 2—Schematic illustration of (a) transverse and (b) *z*-direction Charpy specimens with and without segregation features inside.

### III. RESULTS

#### A. Segregation in Slab and Strip

Figures 3(a) and (b) show the macro-etched slab images of steels #1 and #2, respectively. It can be seen that there are larger and more severe segregated features in slab #1 compared to that of #2, supporting the higher segregation rating of slab #1. In addition, the percentages of segregated features were calculated by dividing the total accumulated length of the segregated features by the image length. The values for slabs #1 and #2 were 25 and 13 pct, respectively, as listed in Table II. The percentage of segregated features for the standard Mannesmann level 2 image was measured to be 24 pct, which is quite close to the percentage of slab #1, indicating that our assessment method is reliable.

Complete full-width transverse sections of the hot-rolled strips for the two materials were quantified by sectioning the cross-section into small pieces and examined following metallographic preparation to reveal the segregation features. These segregated features which appeared as dot pattern in the slabs were now in the form of stringers. Examples of the etched

strip images are shown in Figures 3(c) and (d). It can be seen from these two images that the stringers in strip #1 were longer compared to those in #2. The sizes of these stringers were measured and the percentage of segregated features for the strips was calculated by the same method as that for the slabs and it was 21 and 10 pct for strips #1 and #2, respectively. It is worth emphasizing that the segregation features are discontinuous in the hot-rolled strips.

The microstructure of the base metal has been taken from strip #1 and it consists of mainly polygonal ferrite with small fractions of pearlite, as can be seen in the optical micrograph and the SEM image presented in Figures 3(e) and (f), respectively. The base metal microstructure of strip #2 is the same as that of #1.

Figures 4(a), (c) and (b), (d) show the optical micrographs of the most segregated regions of the strips #1 and #2, respectively. It can be seen that the segregation band in strip #1 is a thick solid black line, while that in strip #2 is lighter in color and is not solid. The black-colored features are pearlite structures. It can be concluded from the micrographs that strip #1 is more severely segregated.



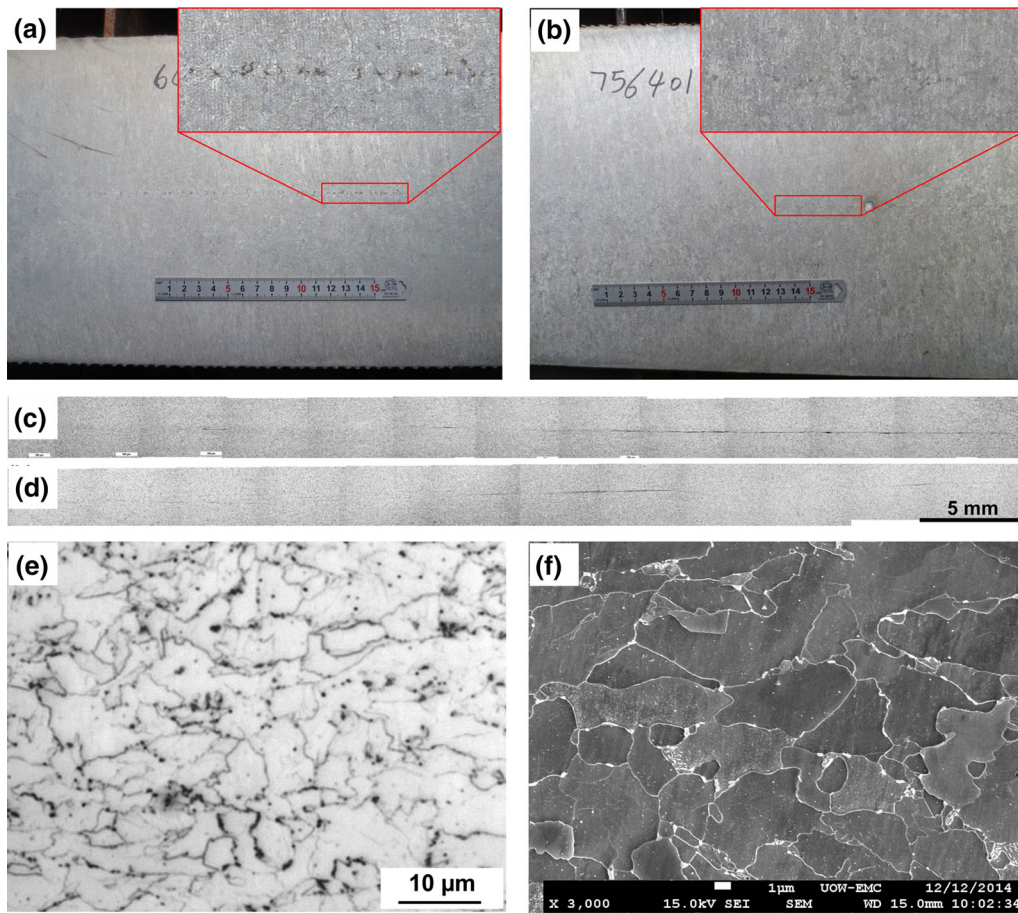


Fig. 3—Macro-etched slab images of samples (a) #1 and (b) #2, selected low-magnification images of etched strips of samples (c) #1 and (d) #2, and high-magnification (e) OM and (f) SEM images of base metal.

**Table II. Measured Percentages of Segregated Features in Slab and Strip**

Sample	Slab (Pct)	Strip (Pct)
#1	25	21
#2	13	10
M2	24	

### B. Transverse CVN Impact Test

A total of 6 transverse Charpy tests were performed on each strip. The results are shown in Figure 5. The Charpy energies for strip #1 ranged between 180 and 225 J, whereas that for strip #2 ranged between 205 and 221 J. The scatter of Charpy impact toughness is 45 J for strip #1 and 16 J for strip #2.

The fracture surface for the lowest energy specimen of #1 shows a line in the middle of the fracture surface, whereas the specimen with the highest energy of #1 and the specimen with the lowest energy in #2 show no line in the middle, as can be seen in Figure 5. All the fracture surfaces show ductile fracture with 100 pct fibrosity.

The two specimens with the lowest Charpy energies in strips #1 and #2 were selected to investigate the fracture surfaces and they will be mentioned as sample T1 and

T2 in the following text. The fracture surfaces of the two samples are presented in Figures 6 and 7. The fractured samples were also sectioned along the midplane perpendicular to segregation line (marked by the dashed lines in the fractographs of sample T1 and T2 in Figure 5) to observe the segregation line.

Figure 6 shows the detailed analysis of the fracture surface for sample T1. It can be seen in Figure 6(a) that the fracture surface has a line in the middle of the surface. Referring to the specimen geometry illustrated in Figure 2(a), it can be seen that the position of the line in the fracture surface is in the same plane as the position of the segregation line in the rolled strip. Further, it can be inferred that the line in the fracture surface is caused by centerline segregation. Figure 6(b) shows an enlarged image at the middle of the fracture surface and it can be seen that the morphology of the midline appears to be different compared to the surrounding regions and the material is elongated toward both sides due to greatly elongated dimples. Figure 6(c) shows a higher magnified view of the midline where broken inclusions can be observed. EDS mapping of the inclusions indicates that these are MnS inclusions. Figure 6(d) shows the optical micrographs of the cross-sectional area beneath fracture surface obtained by cutting the fractured specimen in the midplane perpendicular to segregation line. A shallow

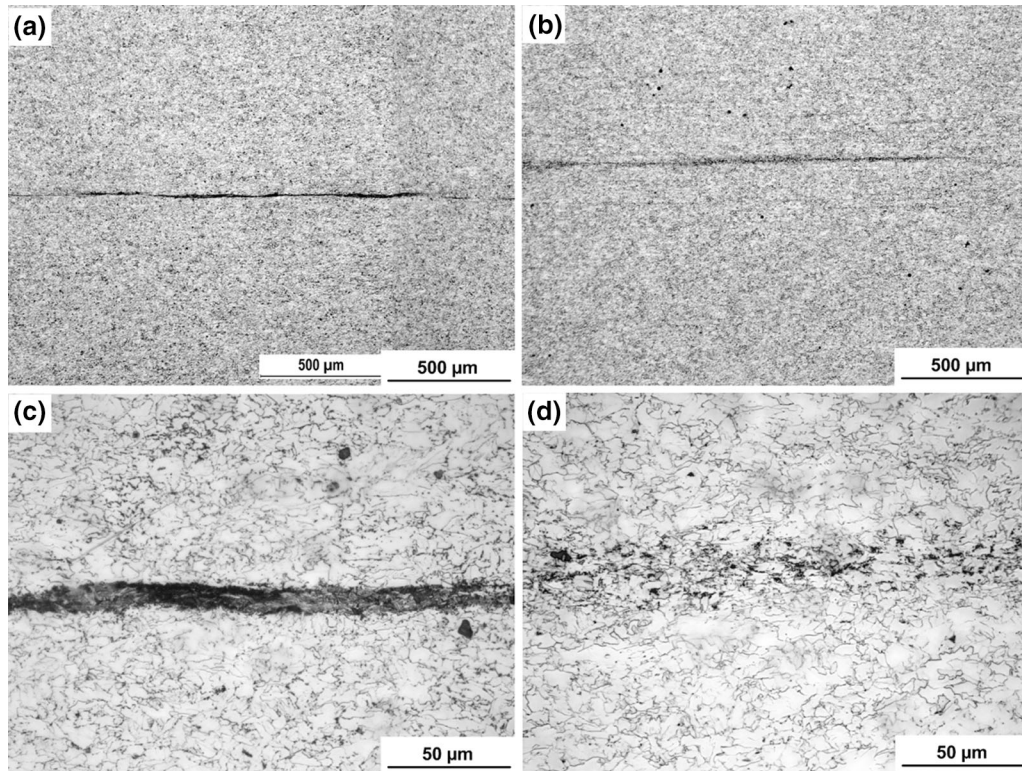


Fig. 4—Optical micrographs of the most segregated regions of the etched strips of (a) and (c) sample #1, and (b) and (d) sample #2.

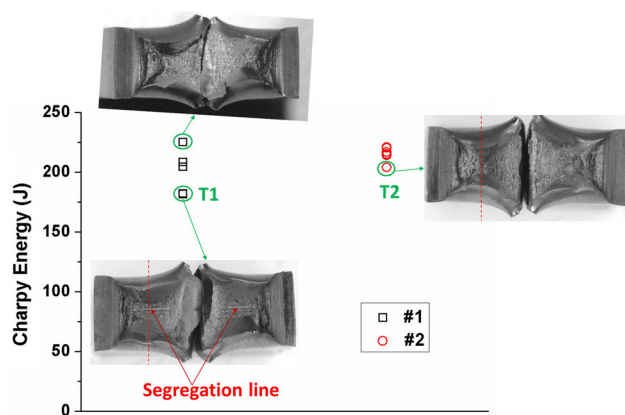


Fig. 5—Transverse Charpy impact results of the two investigated hot-rolled strip steels, carried out at 293 K (20 °C).

valley is observed at the position of the line shown in Figure 6(a). An enlarged image close to the center region of the fracture surface shows lines of pearlite structure. It confirms the speculation above that the centerline segregation is the reason for the line in the fracture surface.

Figure 7 shows the analysis of the fracture surface for sample T2. Figure 7(a) presents the general appearance of the fracture surface which is ductile fracture and without any line in the sample compared to that of sample T1. An enlarged micrograph in the middle of the fracture surface (Figures 7(b) and (c)) only shows large

and small dimples which are typical of ductile fracture, but without any inclusions like in Figure 6(c). The cross-sectional image (Figure 7(c)) does not show any pearlite structure band in the mid-thickness line.

Figure 8 presents more detailed views at the midline of the transverse fracture surfaces from strip #1. Figure 8(a) shows a large but shallow elongated dimple that nucleated at the center and elongated toward the right of the image. There can be seen many fragmented MnS inclusions at the bottom of the shallow dimple (Figure 8(b) shows the MnS inclusions at a larger magnification). It can be inferred that void nucleated at these MnS inclusions and then grew toward both sides to form these elongated dimples. Even at a higher magnification view, brittle fracture was not identified at the midline, as can be seen in Figure 8(c). After etching the fracture surface using 2.5 pct nital for 100 seconds, most of the pearlite structure at the midline has been removed and brittle fracture patterns appear like intergranular fracture at the midline has been revealed, as can be seen in Figure 8(d).

### C. Z-Direction CVN Impact Test

Figure 9 shows an example of the prepared z-direction Charpy specimen from strip #1 with centerline segregation in the specimen. It can be seen in Figure 9(a) that there are some voids in the welds. This is because the welding heat input was restricted to ensure that there is sufficient distance between the weld heat-affected zone (HAZ) and the centerline of the specimen to ensure that



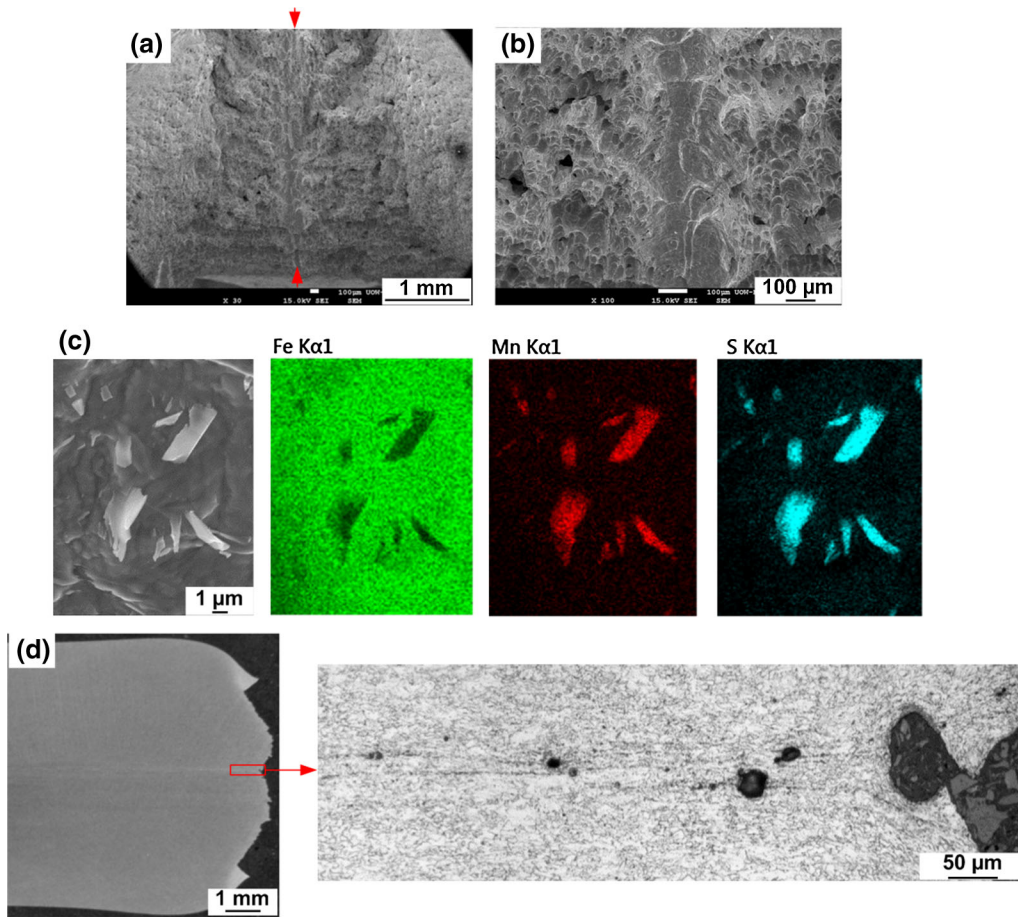


Fig. 6—(a) SEM fractographs of fracture surfaces of sample T1, (b) enlarged view of the center region, (c) EDS mapping of the center region at high magnification, and (d) optical micrographs of the cross-sectional area beneath the fracture surface.

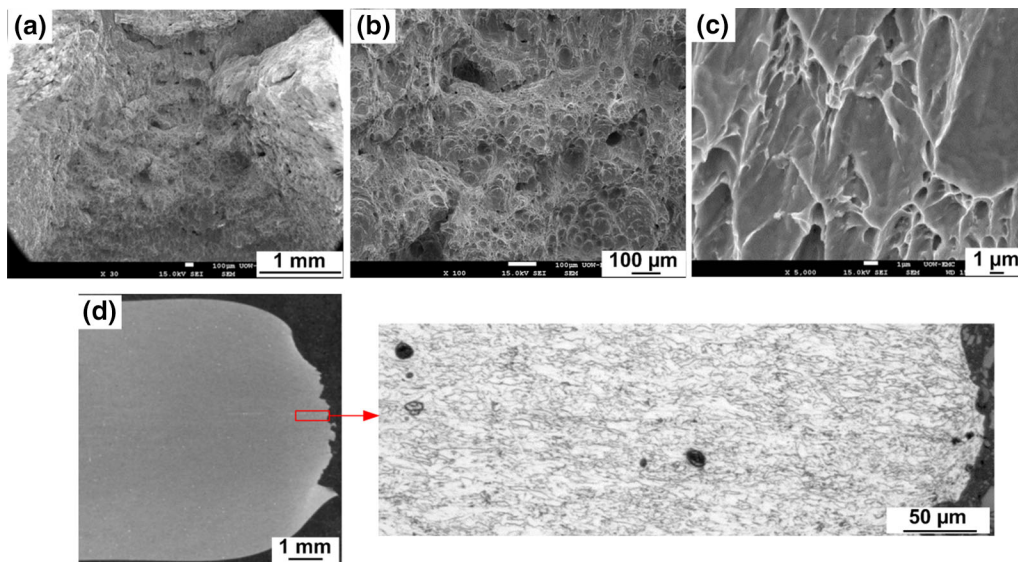


Fig. 7—(a) SEM fractographs of fracture surfaces of sample T2, (b) and (c) enlarged view of the center region, and (d) optical micrographs of the cross-sectional area beneath the fracture surface.

the stud welding procedure did not change the microstructure at the center of the strip. Close examination of the centerline segregation shows a thick

pearlite structure as can be seen in Figures 9(b) and (c). The hardness in the pearlite band is  $HV\ 235 \pm 10$  and in the ferrite matrix is  $HV\ 170 \pm 4$ . It is assumed

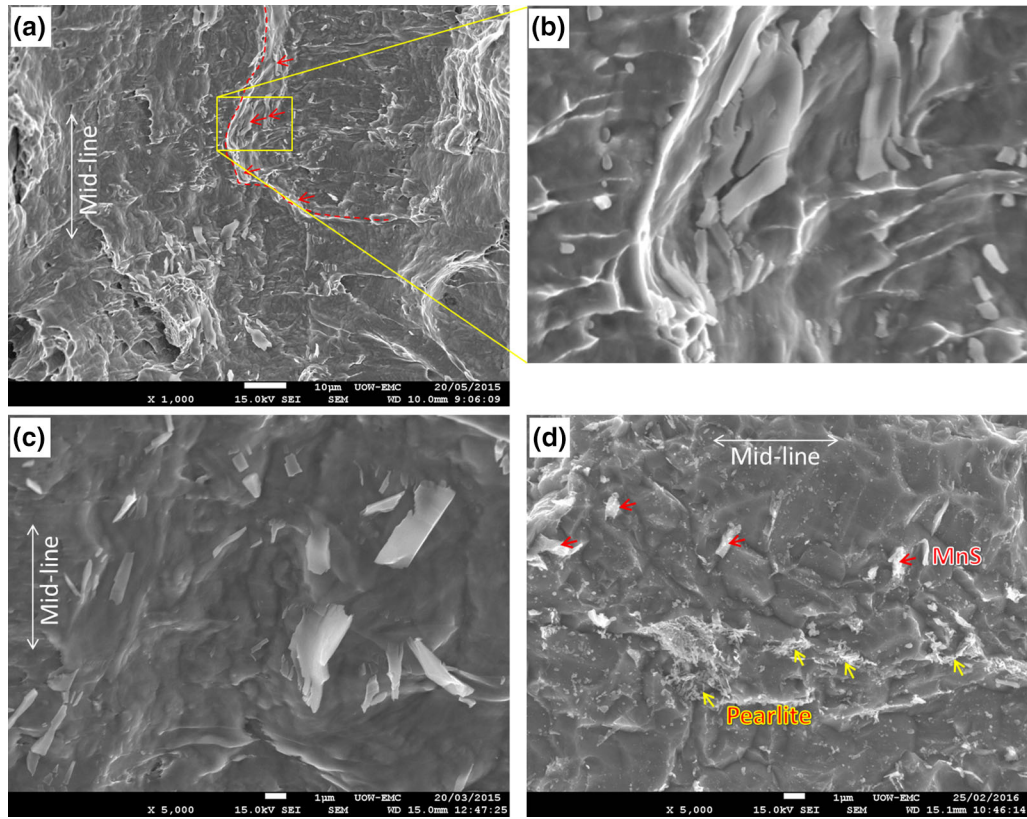


Fig. 8—SEM fractographs at the midline of the fracture surfaces from strip #1, (a through c) as-Charpy fractured, and (d) after etching by 2.5 pct nital for 100 s. Note that the direction of the midline for (d) is different from (a through c).

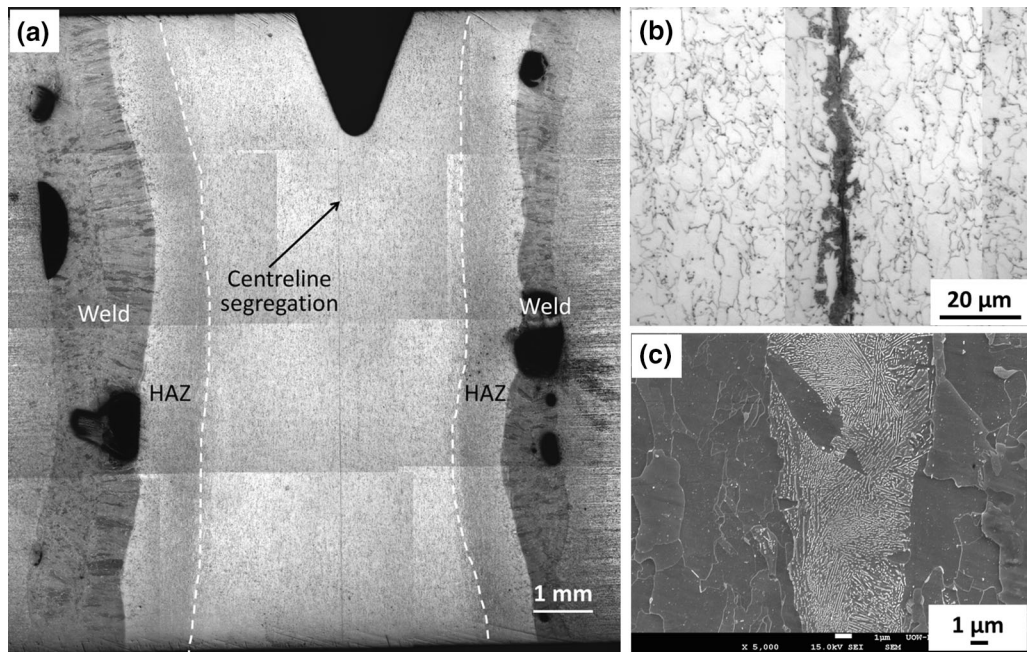


Fig. 9—An example of the prepared z-direction Charpy V-notch impact specimen with segregation line close to notch tip: (a) overall view and (b) and (c) enlarged view at the center region of (a).

that the fracture will occur at the midplane with pearlite structure during CVN impact test. It should be noted that although some voids exist in the welds, there was no

visible deformation along the welds during CVN impact test. All of the Charpy failed specimens were carefully checked to ensure that.



A total of 7 *z*-direction Charpy tests were performed on each strip. Figure 10 shows the *z*-direction CVN impact test results. The Charpy energies for strip #1 ranged between 60 and 235 J, whereas those for strip #2 ranged between 209 and 234 J. There is a much larger scatter of Charpy impact toughness for strip #1 than for strip #2.

The fracture surface for the highest energy specimen of #1 shows ductile fracture with 100 pct fibrosity (Figure 10(a)). The ones with lower energies show some fraction of cleavage at the fracture surface and the lower the Charpy energy, the larger the fraction of cleavage at the fracture surface. The fracture surfaces of #2 generally show ductile fracture with the exception of some samples where a small fraction of cleavage was observed. Most of the specimens were not fully broken at the end of the tests. The exceptions were the two specimens with the lowest Charpy energy (61 and 78 J) of #1, which were fully broken after the tests.

Two specimens from strip #1 which showed almost full cleavage and half cleavage were selected to investigate the fracture surfaces and they will be referred to as samples Z1a and Z1b in the following text. One specimen from sample #2 which showed a small fraction of cleavage was further investigated and will be named Z2.

Before CVN impact test, the specimens were polished and etched, and the regions close to Charpy notch for the samples Z1a and Z2 are shown in Figures 10(d) and (g), respectively. It can be seen that there is a segregation line close to the notch of Z1a (marked by small red arrows) but not for Z2. No segregation line was observed for Z1b either but the image is not shown. The broken Charpy specimens for Z1a, Z1b, and Z2 are shown in Figures 10(e), (b), and (h), respectively. The

brittle fracture regions are indicated by the enclosed yellow dash lines. The fractured specimens of Z1a, Z1b, and Z2 were cut along the red dashed lines to observe the cross-sections of the fracture surfaces. The cross-sections of the three specimens are presented in Figures 10(f), (c), and (i), respectively. Cleavage fracture is flat and appears as straight lines in the cross-sections.

It should be noted that the cleavage plane of the specimen Z1a is not perpendicular to the side of the specimen (Figure 10(f)). The reason is due to the misplace of notch tip with respect to the segregation line and the segregation line not perpendicular to the side of the specimen either due to machining inaccuracy or due to segregation line not exactly in the centerline of the strip. It can be seen in Figure 10(d) that the segregation line is located to the left side of the notch tip and is not perpendicular to the side of the specimen. Consequently, the cleavage fracture surface formed by fracture propagation along the segregation plane is not perpendicular to the side of the specimen. Due to the misalignment of the segregation line and the notch tip, and the fact that the segregation line is not perpendicular to the side of the specimen, the measured energy overestimates the fracture energy that would have been spent if the specimen had broken in pure opening mode.

The instrumented load–displacement curves of samples Z1a, Z1b, and Z2 are shown in Figure 11. It can be seen that the three curves coincide with one another before the displacement reaches ~4 mm, where sample Z1a experienced a sharp jump which appeared to be the same as brittle crack jump described in Reference 17. The sharp jump phenomenon occurred at a later stage for sample Z1b (~12 mm displacement) after a certain distance of ductile crack propagation. For sample Z2, the sharp jump was also observed, but at a much later

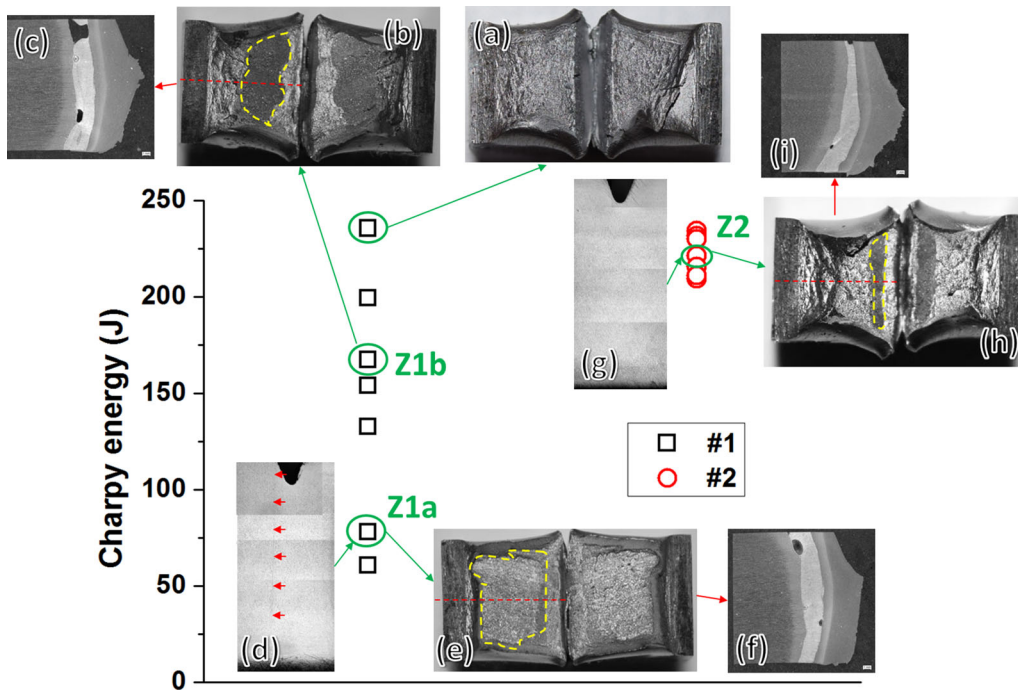


Fig. 10—*Z*-direction Charpy impact results of the two investigated hot-rolled strip steels, carried out at 293 K (20 °C).



stage (~17 mm displacement) the magnitude was much smaller than samples Z1a and Z1b. After the sharp jump, a consequent ductile final rupture was observed for all three samples. All load values became 0 at displacement of 28 mm. The areas under the curves increase from sample Z1a to Z1b to Z2, indicating the increasing toughness. As indicated in the embedded table in Figure 11, the Charpy impact toughness for Z1a, Z1b, and Z2 is 78 J, 167 J, and 225 J, respectively.

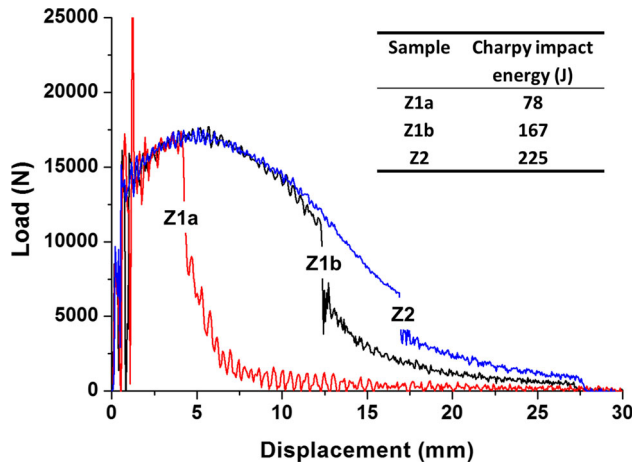


Fig. 11—Load–displacement curves of three selected *z*-direction Charpy specimens Z1a, Z1b, and Z2.

The fractographs of samples Z1a, Z1b, and Z2 are shown in Figures 12 through 15. It can be seen from the figures that the fracture surfaces of the three samples are quite different from one another. Figure 12 shows the fractographs of sample Z1a which appear as a brittle cleavage fracture surface with minimum necking and is overall flat. Closer examination of the fracture surface reveals three types of structures: cleavage facets containing river markings, ductile tearing ridges between the facets and long, rod-shaped features. EDS mapping of the fracture surface confirmed that the rod-shaped features were MnS inclusions, as indicated in Figure 13.

Figure 14 shows the fracture surfaces of sample Z1b. It can be seen that the fracture surface can be separated into two regions: ductile fracture region on top close to the original notch and brittle fracture region on the bottom. The brittle fracture region is slightly larger than the ductile fracture region. The brittle fracture region is also flat, the same as the fracture surface of sample Z1a. There can be seen apparent necking and the shear lip areas are larger than sample Z1a. Closer examination of the fracture surface reveals large and small shearing dimples and microvoids in the ductile region, as can be seen in Figure 14(c). The brittle fracture region shows a similar appearance as sample Z1a with cleavage facets, shear ridges, and MnS inclusions, as can be seen in Figure 14(d).

Figure 15 shows the fracture surfaces of sample Z2. It can be seen that the fracture surface is rough in

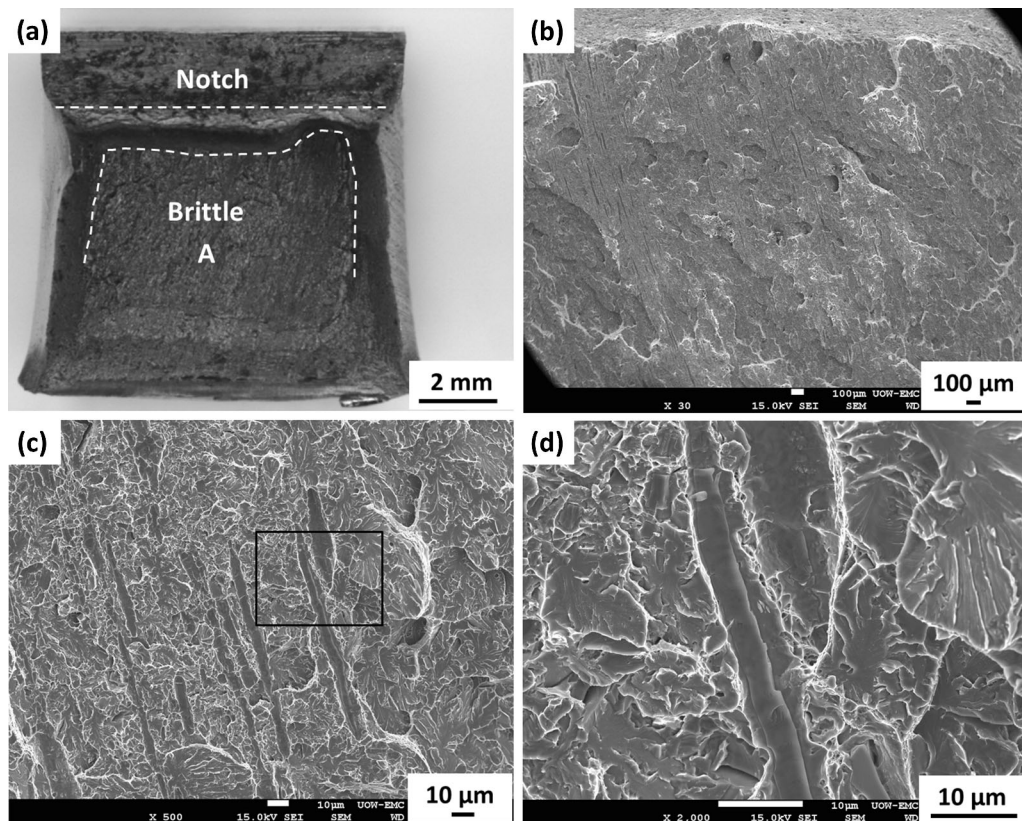


Fig. 12—Fractographs of fracture surfaces of sample Z1a: (a) overall view, (b) SEM at low magnification, (c) enlarged view at position A in (a), and (d) enlarged view of the frame in (c).

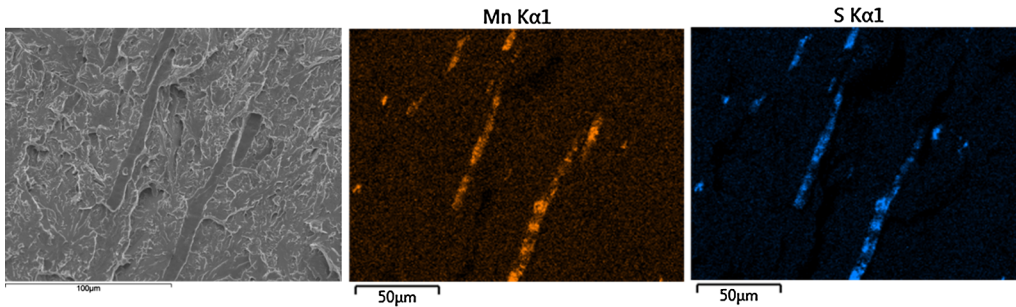


Fig. 13—EDS mapping at the fracture surface of sample Z1a.

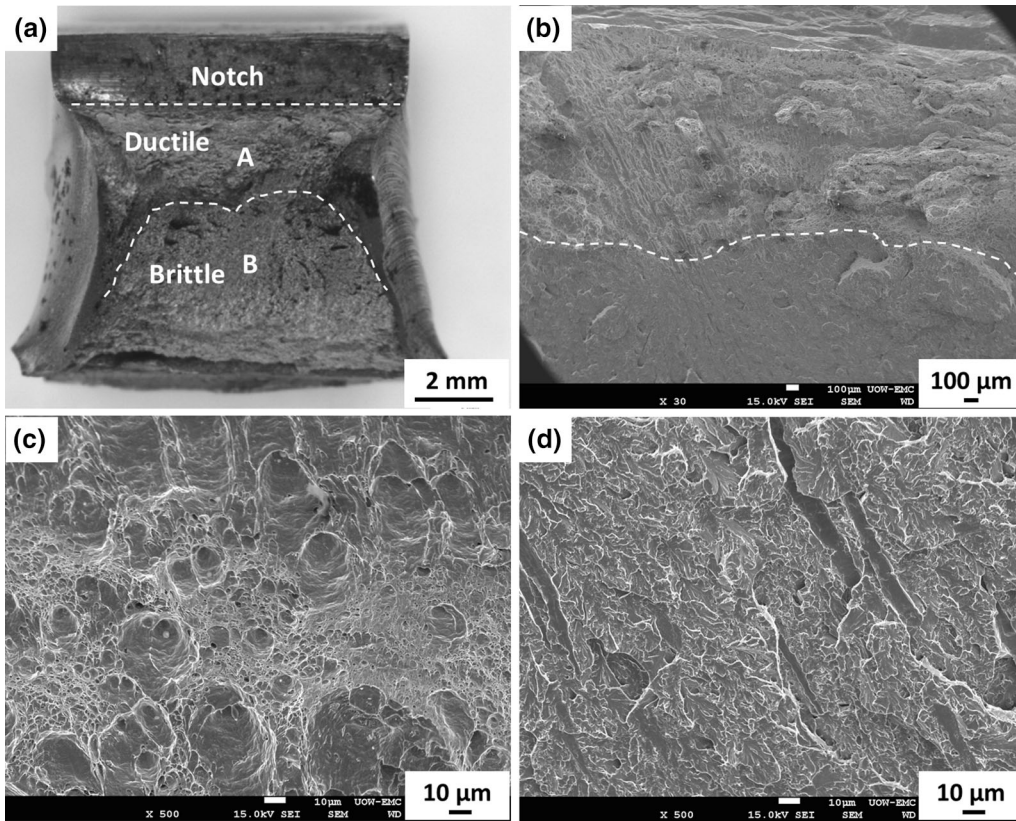


Fig. 14—Fractographs of fracture surfaces of sample Z1b: (a) overall view, (b) low-magnification SEM at center region, (c) enlarged view at position A in (a), and (d) enlarged view at position B in (a).

appearance and the amount of necking is maximum among the three samples. It can also be separated into two regions similar as in sample Z1b, but the brittle fracture region is much smaller in area. Closer examination of the ductile region reveals large and small shearing dimples and microvoids similar as in the ductile fracture region of Z1b, as can be seen in Figure 15(c). The brittle fracture region shows only cleavage facets, as can be seen in Figure 15(d).

Figure 16(a) presents the relationship between the area fraction of brittle fracture and Charpy impact energy of  $z$ -direction Charpy test results. The data points are from all the specimens of strip #1 and specimen Z2. It can be seen that with decreasing Charpy impact energy, the brittle fracture area fraction

increases and the relationship is linear in general. Figure 16(b) presents the relationship of the area fraction of MnS inclusions and Charpy impact energy of specimens Z1a, Z1b, and Z2. It shows that with increasing area fraction of MnS inclusions, the Charpy impact energy decreases.

## IV. DISCUSSION

### A. Centerline Segregation in Strips

In the current work, centerline segregation appears as many individual pockets along the centerline for both investigated slabs, as can be seen in Figure 3(a). The difference between the two slabs is that the pockets are



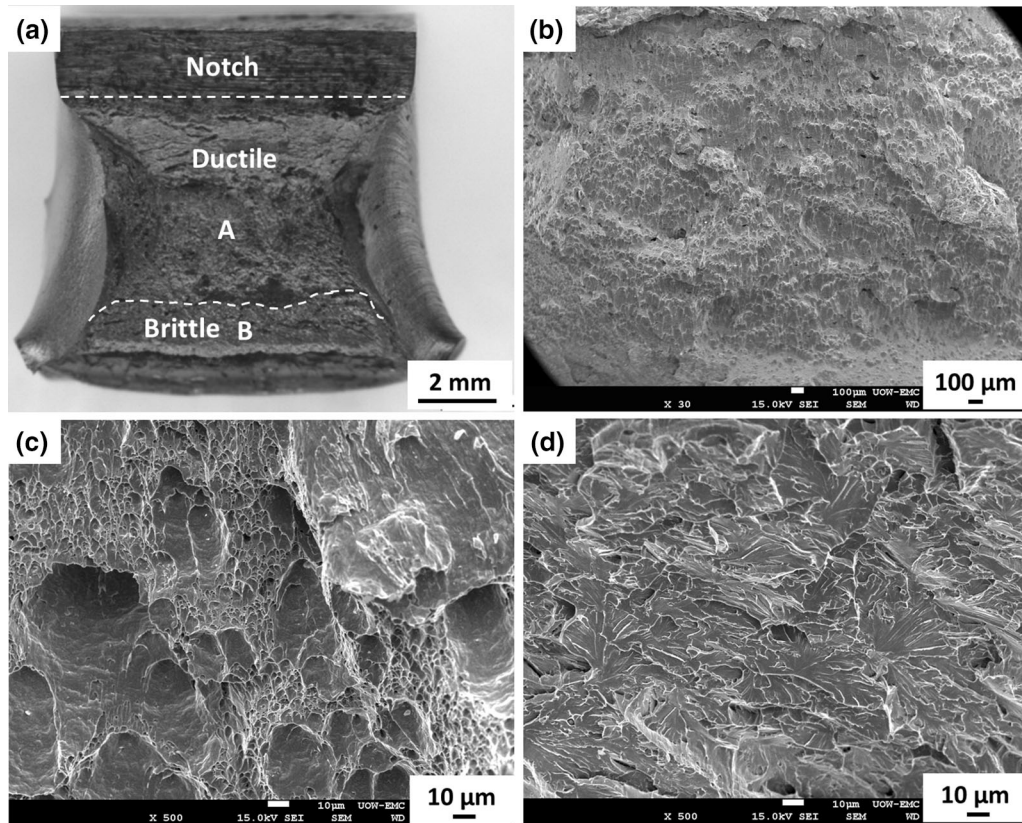


Fig. 15—Fractographs of fracture surfaces of sample Z2: (a) overall view, (b) low-magnification SEM at center region, (c) enlarged view at position A in (a), and (d) enlarged view at position B in (a).

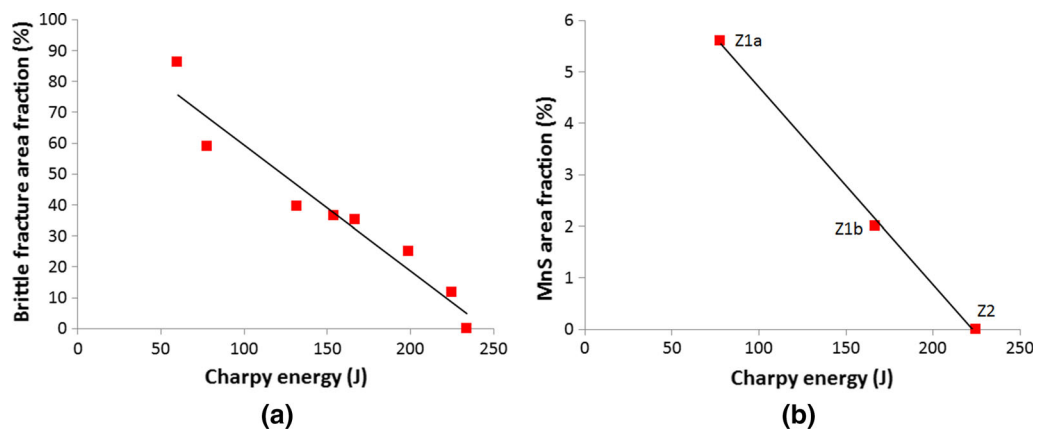


Fig. 16—Relationship between (a) brittle fracture area fraction and (b) MnS area fraction and Charpy impact energy.

darker and larger for slab #1. During hot rolling of continuously cast slabs, the individual segregation pockets will be rolled out to become thin, elongated line features in the mid-thickness of the rolled strips. The segregation lines may be relatively long or short depending on the size of the original segregation pockets, but there are quite large gaps between the segregation lines.

The segregation percentages of the standard Mannesmann charts are 0, 24, 45, 86, and 90 pct, respectively, for the level 1 to 5 images. It is evident that the relationship of the segregation percentages and

Mannesmann ratings is not linear. There is a sudden increase from level 3 to level 4. The segregation percentages of the current investigated slabs were 25 and 13 pct and were rated as 2.0 and 1.4 based on Mannesmann ratings. The ratings were reasonable as compared to the segregation percentages of the Mannesmann charts.

The segregation percentages in related strips, however, cannot be compared with any published result as none have been quantitatively reported. These values are slightly less than the segregation percentages of corresponding slabs because some of the small segregated

pockets were very light in color and cannot be distinguished from the metal matrix after hot rolling. Nevertheless, the segregation percentages in hot-rolled strips were in accordance with those in slabs.

Comparing the most segregated regions in strips #1 and #2 (Figure 4), it can be seen that even for small differences in segregation ratings, like in current case 2.0 and 1.4, there is still a noticeable difference in segregation severity. The segregation band in strip #1 is a solid black line composed of pearlite band, while that in strip #2 is composed of pearlite islands scattered at the centerline region. The segregation bands in rolled strips are discontinuous, especially for the current case where the segregation ratings are low. For high segregation ratings such as 4 or 5, the segregation bands in rolled strips/plates would be thicker and more continuous, as the segregation features in slabs are more continuous and high in percentage (~90 pct). However, it is difficult to assess real samples with such high segregation ratings, since in modern continuous casting, the casting machine is maintained in good conditions that slabs with thus high segregation ratings are rarely produced.

### B. Influence of Centerline Segregation on Charpy Impact Toughness

Although it is known that centerline segregation can result in lower Charpy impact toughness, Charpy impact testing of strips/plates rolled from slabs with known segregation ratings have rarely been reported. Reference 5 reported the influence of centerline segregation on product properties by comparing two different materials. Although segregation ratings were not given, it can be roughly assessed based on the macro-etched images in the paper. The segregation ratings were 1.2 and 2.0 based on our rating method. It was reported in the paper that the toughness value at the center of the plate from segregation 1.2 slab was improved by 20 pct compared to the value of the plate from segregation 2.0 slab. This is in accordance with the less scattered and slightly higher average values of Charpy impact toughness observed in the low segregation rating strip in the current work.

When discussing the influence of centerline segregation on local mechanical properties such as Charpy impact toughness, it is worth emphasizing that the segregation features in rolled strips are discontinuous, especially for low segregation rating materials. Thus, not all specimens contained segregation features, and consequently only a fraction of the specimens have lower Charpy energies, as can be seen in Figures 5 and 10. What the segregation rating really influences is the scatter or the lowest possible value of Charpy impact toughness. It can be seen in Figures 5 and 10 that the specimens from higher segregation rating slab #1 have a larger scatter. Further #1 has the lowest impact energy value compared to #2. Therefore, it is more reasonable to conclude that the strips rolled from higher segregation level slabs are more likely to exhibit greater variability in Charpy impact toughness.

It should also be noted that many z-direction specimens showed partial brittle fracture surfaces. Specimen

Z1b and other specimens from strip #1 that have Charpy impact energies between 100 and 200 J are examples. Before Charpy test, segregation lines were either not observed or only observed in small regions for these specimens. Brittle fracture for all these specimens was observed following initial ductile fracture. It is not clear whether the observed brittle fracture surfaces represent all segregated regions in the specimens. There are also chances that for some specimens, brittle fracture may not occur because the notch of the specimen has not been placed in the center region or the segregation is distant from fracture propagation path since the segregation line is not always straight and there may be a few segregation lines at different thickness positions. In any case, the measured Charpy impact energy tends to overestimate the fracture energy of the segregated specimens.

The hardness values of the pearlite band in strip #1 and pearlite islands in strip #2 are  $HV\ 235 \pm 10$  and  $221 \pm 11$ , respectively. This is in agreement with the Reference 4 that the segregation bands that correspond to higher segregation levels in slabs have higher hardness and concomitantly lower Charpy impact toughness in hot-rolled strips.

It is worth mentioning that even though the effect of segregation on Charpy impact toughness is clear, the difference in Charpy energy of the two strips may be insignificant in terms of structural performance. This is because the segregation levels of the investigated steels are low (less than or equal to level 2 based on Mannesmann standard level 1 to 5). The US Department of Transportation Pipeline and Hazardous Materials Safety Administration (DOT PHMSA) suggests that the acceptance level for centerline segregation is Mannesmann level 1 or 2 for general use and Mannesmann level 1 for sour service pipe and center-slit pipe. According to this recommendation, the current investigated steels are both acceptable for all applications except for sour service and center-slit pipe. Therefore, it is understandable that the Charpy impact toughness for the investigated strips remains high for the transverse Charpy test. Thus, from the results of the current work, it is paramount that samples with segregation level 3 and above should be investigated.

### C. Transverse vs z-Direction CVN Impact Test

The current transverse CVN test results generally agree with the results shown in Reference 18 with the exception of the lines (or shallow valleys) with MnS inclusions observed for the lower Charpy impact toughness samples (sample T1). The metal matrix at the line/valley shows ductile fracture, which means that even though the pearlite band at the centerline has some influence on the transverse Charpy properties, the influence is not as severe as other structures like a martensite band or a bainite band, where brittle fracture at the segregated bands were observed for tests at room temperature.<sup>[19,20]</sup>

The z-direction CVN test results of strip #1 show a large scatter in Charpy impact toughness and brittle fracture on lower energy samples, which is not often



observed for test at room temperature. The quasi-cleavage fracture characteristics and the Charpy energy as low as 60 J suggest that the test temperature should be close to the lower shelf of Charpy transition curve, which is much higher than the transition temperature at half jump for normal transverse CVN impact test of X65 [−183 K (−90 °C)].<sup>[18]</sup> This suggests that the transition temperature of the *z*-direction Charpy test is significantly higher than that of the transverse test. It is in accordance with the results in Reference 11.

It should be noted that there is anisotropy in Charpy impact toughness between the transverse and *z*-direction test results. Since the *z*-direction results for strip #1 are highly scattered, the results for strip #2 are used in the following discussion. The average values of the measured Charpy impact toughness for transverse and *z*-direction specimens are  $215 \pm 6$  and  $225 \pm 13$  J, respectively. However, the transverse Charpy specimens are subsized, whereas the *z*-direction specimens are full sized. Considering this size effect and assuming that the Charpy energy vs specimen thickness relationship is linear, the estimated Charpy impact toughness for full-sized transverse specimens is  $287 \pm 8$  J. This is much higher than the toughness tested from *z*-direction. The reason may be attributed to two aspects: the centerline segregation and the texture. Although the segregation in strip #2 is weak and brittle fracture was rarely observed for the *z*-direction specimens of strip #2, the segregation plane may still decrease the Charpy impact toughness when tested from *z*-direction. Besides, hot-rolled steels are strongly textured. In the current case, typical rolling texture composed of  $\alpha$  fiber and  $\gamma$  fiber was observed in strip #2. The texture may also contribute to the anisotropy of toughness in transverse and *z*-direction.

#### D. MnS Inclusions

According to Reference 11, splitting in transverse samples will occur by delamination along planes or interfaces in a laminated structure which have a lower fracture stress than the stress required for transverse fracture. It is evident from the hardness test results that the pearlitic band structure was harder than the ferrite matrix. The pearlite band, therefore, can serve as a possible low fracture stress plane or interface where delamination can occur. Although in the current experiment only a shallow valley was observed (Figure 6(d)), which was more appropriate to be referred to as mild lamellar tearing than splitting, it shows that this center plane was a low fracture stress plane. It was also claimed in Reference 11 that splitting or lamellar tearing is usually related to the planar orientation of highly segregated inclusions, which in the current study would be MnS inclusions.

MnS is a common type of inclusions that forms during the solidification of steel.<sup>[21–23]</sup> Although the S content is 0.002 pct in the investigated steel, it is difficult to avoid the formation of MnS inclusions, even in Ca-treated steel, in the central segregated regions of the slab. Upon hot rolling, the MnS inclusions elongate along the rolling direction to the form of stringers. MnS

appears as broken rod pieces in Figure 6 and long rod shaped in Figures 12 through 14.

Centerline segregation can have a deleterious effect on Charpy impact toughness.<sup>[4–9]</sup> It has also been reported that a high volume fraction of MnS inclusions can decrease the impact toughness of steel.<sup>[22,24]</sup> Comparing Figure 6 with 7, it is logical to assume that the line observed in sample T1 and its lower Charpy impact toughness were caused by the pearlite structure in the mid-thickness plane (*i.e.*, centerline segregation) and the MnS inclusions located in the same plane. Comparing Figures 12, 14, and 15, it can be inferred that the brittle fracture surface and the rod-shaped MnS inclusions were responsible for the lower Charpy impact toughness of samples Z1a and Z1b. Since the pearlite band and MnS inclusions seem always to be observed at the same location in the same mid-thickness plane, it is safe to say that the mid-thickness plane is the weakest plane in the strip. Therefore, it can be concluded that centerline segregation and the MnS inclusions both have contributed to the lower Charpy energy for sample T1.

An exception is that MnS inclusions were not observed in the small area of brittle fracture in sample Z2. The brittle fracture itself caused a small load drop (Figure 11) and consequently a slightly lower Charpy impact toughness, but the influence was very minor. It is worth pointing out that MnS inclusions were only observed in strip #1 even though the chemical compositions of Mn and S for the two steels were the same. As both steels, #1 and #2, were Ca treated, the reason for the presence of MnS only in #1 and not in #2 requires further investigations into the secondary steelmaking and the casting production histories of the two steels. It is also reasonable to assume, based on published literature, that P may have also contributed to the lower Charpy impact toughness in strip #1. This will be evaluated and quantified as part of our ongoing research.

## V. CONCLUSIONS

The following conclusions can be derived on the basis of the current investigation of transverse and *z*-direction CVN impact tests on samples from strips hot rolled from continuously cast slabs with different centerline segregation levels.

1. Discontinuous segregated line features which consisted of pearlite structure were observed in strip samples that were hot rolled from slabs with segregation levels 2.0 and 1.4. The segregation fraction in strip samples is in accordance with that found in the corresponding slab samples.
2. Charpy specimens located at segregated regions exhibited lower Charpy impact toughness and strips rolled from higher segregation level slabs are more likely to exhibit greater variability in Charpy impact toughness.
3. For the transverse Charpy tests, a lower Charpy impact toughness and a line in the mid-thickness of the Charpy fracture surfaces can be observed if the

Charpy specimens were located at segregated regions. MnS inclusions were observed in the linear feature.

4. For *z*-direction Charpy tests, a lower Charpy impact toughness and brittle fracture surface with cleavage facets and rod-shaped MnS inclusions were observed for strip #1 if the Charpy specimens were located at segregated regions.
5. The centerline segregation and MnS inclusions have contributed to the lower Charpy energy observed.

## ACKNOWLEDGMENTS

The authors would like to thank Baosteel-Australia Joint research and development Centre (BAJC) for its financial support. The Energy Pipelines CRC (EPCRC), supported through the Australian Government's Cooperative Research Centres Program, is also acknowledged for its in-kind support.

## REFERENCES

1. C. Beckermann: *ASM Handb.*, 2008, vol. 15, pp. 348–52.
2. J.M. Gray, C.C. Chen, S.V. Subramanian, P.A. Peters and T. Abbott: Report No. L51759, Pipeline Research Council International, Technical Toolboxes, Inc. Houston, Texas, July 1996.
3. Report No. SN 960, SMS Demag AG Mannesmann, February 2009.
4. R. Mendoza, M. Alanis, R. Perez, O. Alvarez, C. Gonzalez, and J.A. Juarez-Islas: *Mater. Sci. Eng. A*, 2002, vol. 337, pp. 115–20.
5. S. Ueyama, M. Niiizuma, and K. Yonezawa: *Nippon Steel Tech. Rep.*, 2013, vol. 104, pp. 102–08.
6. I.D. Simpson, L.G. Moore, and C.L. Carey: *Ironmak. Steelmak.*, 2003, vol. 30, pp. 158–64.
7. I.D. Simpson, Z. Tritsiniotis, and C.L. Carey: *La Metall. Italiana*, 1992, vol. 84, pp. 599–605.
8. A.S. Bor: *ISIJ Int.*, 1991, vol. 31, pp. 1445–46.
9. T. Kyada, J.R. Shant, R.K. Goyal, and T.S. Kathayat: *J. Mater. Metall. Eng.*, 2014, vol. 4, pp. 31–39.
10. J.M. Gray: *International Technology Conference Azov Steel 2000-Rolled Steel Plates for Large Diameter Oil and Gas Pipelines and Critical Structural Applications*, Mariupol, Ukraine, 2002.
11. C. Grobler: *Weldability Studies on 12 % and 14% Chromium Steels*, University of Pretoria, South Africa, 1987.
12. B. Mintz: *Met. Technol.*, March 1980, pp. 127–29.
13. G. Baldi and G. Buzzichelli: *Metal Sci.*, 1978, vol. 12, pp. 459–72.
14. L.H. Su, H.J. Li, C. Lu, I. Simpson, F. Barbaro, L. Fletcher, L. Zheng, M.Z. Bai, J.L. Shen, L.Q. Fan, GD Xu, and GZ Gui: *6th International Pipeline Technology Conference*, Belgium, Ostend, 2013, pp. S27–01.
15. L.H. Su, H.J. Li, C. Lu, J.T. Li, I. Simpson, F. Barbaro, L. Fletcher, L. Zheng, M.Z. Bai, J.L. Shen, L.Q. Fan, G.D. Xu and G.Z. Gui: *Energy Materials 2014, TMS, Xi'an*, pp. 575–81.
16. International Organisation for Standardisation, ISO 148-1, 2009.
17. V.V. Kharchenko, E.A. Kondryakov, V.N. Zhmaka, A.A. Babutskii, and A.L. Babutskii: *Strength Mater.*, 2006, vol. 38, pp. 535–41.
18. G. Pluinage, M.B. Amara, J. Capelle, and Z. Azari: *Proced. Mater. Sci.*, 2014, vol. 3, pp. 1560–65.
19. M.M. Salama: *Trans. ASME*, 2004, vol. 126, pp. 346–49.
20. R. Feng, S. Li, X. Zhu, and Q. Ao: *J. Alloys Compd.*, 2015, vol. 646, pp. 787–93.
21. S. Maropoulos and N. Ridley: *Mater. Sci. Eng. A*, 2004, vol. 384, pp. 64–69.
22. A. Ghosh, S. Sahoo, M. Ghosh, R.N. Ghosh, and D. Chakrabarti: *Mater. Sci. Eng. A*, 2014, vol. 613, pp. 37–47.
23. Y. Tomita: *Metall. Trans. A*, 1988, vol. 19A, pp. 1555–61.
24. D.K. Biswas, M. Venkatraman, C.S. Narendranath, and U.K. Chatterjee: *Metall. Trans. A*, 1992, vol. 23A, pp. 1479–92.